Article

pubs.acs.org/Biomac

# Lignin-Based Electrospun Nanofibers Reinforced with Cellulose Nanocrystals

Mariko Ago,[†,‡] Kunihiko Okajima,[‡] Joseph E. Jakes,[§] Sunkyu Park,[†] and Orlando J. Rojas*[,†,∥]

[†]Department of Forest Biomaterials, North Carolina State University, Raleigh, North Carolina 27695, United States

[‡]Faculty of Science and Engineering, Tokushima Bunri University, Sanuki, Kagawa, Japan

[§]Performance Enhanced Biopolymers, Forest Products Laboratory, USDA Forest Service, Madison, Wisconsin 53726, United States

[∥]Department of Forest Products Technology, School of Chemical Technology, Aalto University, FI-00076 Aalto, Espoo, Finland

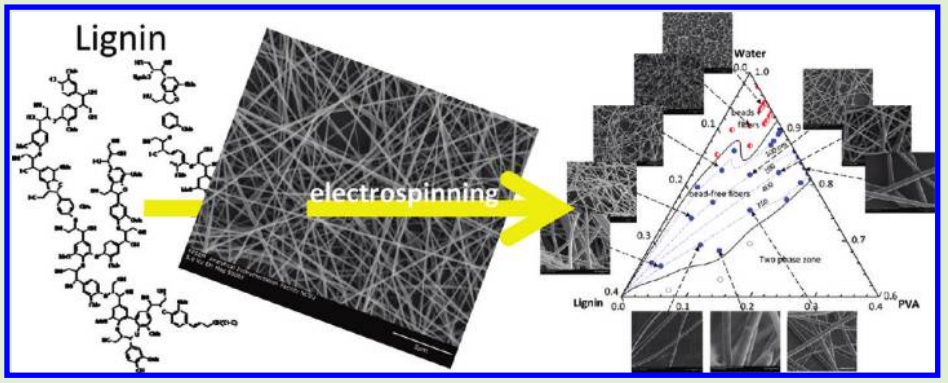


**ABSTRACT:** Lignin-based fibers were produced by electrospinning aqueous dispersions of lignin, poly(vinyl alcohol) (PVA), and cellulose nanocrystals (CNCs). Defect-free nanofibers with up to 90 wt % lignin and 15% CNCs were achieved. The properties of the aqueous dispersions, including viscosity, electrical conductivity, and surface tension, were examined and correlated to the electrospinnability and resulting morphology of the composite fibers. A ternary lignin−PVA−water phase diagram was constructed as a tool to rationalize the effect of mixing ratios on the dispersion electrospinability and morphology of the resulting fibers. The influence of reinforcing CNCs on the thermal properties of the multicomponent fibers was investigated by using thermal gravimetric analysis and differential scanning calorimetry. The thermal stability of the system was observed to increase owing to a strong interaction of the lignin−PVA matrix with the dispersed CNCs, mainly via hydrogen bonding, as observed in Fourier transform infrared spectroscopy experiments.

## INTRODUCTION

Lignin is found as a natural macromolecule in the cell wall of vascular plants, making it one of the most abundant macromolecules in the biosphere, second to cellulose. Lignin has attracted renewed attention given its anticipated role as a byproduct in biorefinery operations and second generation bioethanol from lignocellulose.[1] The use of lignin as a precursor in the fabrication of new materials has been reported.[2] Composites of commercially available kraft or organosolv lignins can be produced after mixing with hydrophilic or hydrophobic polymers, such as polyethylene oxide (PEO),[3] polyvinyl alcohol (PVA),[3,4] polyhydroxybutyrate,[5] polyethylene terephthalate,[3] polypropylene,[3] and polycaprolactone.[6] The obtained resins can be thermally processed into fibers, compostable plastics, and structural materials. Related studies have indicated that lignin possesses an affinity for hydrophilic polymer because of lignin's many polar groups, which include alcoholic and phenolic structures.[7] Kubo et al.[8] reported on the use of kraft and organosolv lignins as precursors for carbon fibers after thermal stabilization and carbonization. Following these efforts, different lignin-based fibers (30−80 $\mu$m diameter) have been produced by melt spinning or extrusion.[9] A commercially available organosolv lignin was electrospun into carbon micro- and nano-fibers, both solid and hollow, by using ethanol and glycerin solutions in a coaxial or triaxial spinneret setup.[10,11] We also reported on the production of fibers based on lignin after electrospinning aqueous solutions of kraft lignin in PEO.[12] More recently, kraft and organosolv lignins were blended with PEO to produce electrospun fibers. Structural and intermolecular interactions, such as hydrogen bonding and association complexes, were proposed as main factors influencing the electrospinnability of these systems.[13]

In electrospinning,[14] extremely rapid solvent evaporation occurs with continued jet flow, resulting in the formation of an outer polymer "skin" and quenching of the polymer matrix macrostructure within a few milliseconds, in a nonequilibrium state.[15−17] Electrospun mats exhibit high porosity and specific surface area, which make them suitable for the production of

Received: December 22, 2011
Revised: January 23, 2012
Published: January 27, 2012

  

high performance materials such as filters, sensors, medical materials, flexible coating, and so on.[18−22] Recently, cellulose nanocrystals (CNCs)[23−25] have made inroads in the production of new materials as reinforcing solid phase in electrospun fibers.[26−30] The high specific surface of CNCs and the available hydroxyl groups suggest the possibility to exploit hydrogen bonding in host matrices to further these initial efforts to produce new materials.

This work describes the manufacture of lignin-based fiber mats produced by electrospinning aqueous dispersions of lignin, PVA, and CNCs. The resulting composite fibers displayed unique and tailorable morphologies and properties. Additionally, they can be considered as a simple model to investigate the nature of intermolecular interactions and their role in structure−property relationships, which could be translated to the more complex natural fibers. PVA was used as an adhesive for cellulose and lignin, the latter of which is a principal component of the fiber matrix. The morphology of the resulting fibers was analyzed via scanning electron microscopy (SEM) and the enhancement of the thermal stability of the electrospun mats by incorporation of CNCs was demonstrated by thermal gravimetric analysis (TGA) and differential scanning calorimetry (DSC).

## MATERIALS AND METHODS

Lignin (kraft lignin from softwood) was obtained from Sigma-Aldrich (St. Louis, MO) with reported molecular weight of 10 kDa (alkali lignin, low sulfur, CAS number 8068-05-1). Poly(vinyl alcohol) (PVA), also from same supplier under trade name Mowiol 20-98 (CAS Number: 9002-89-5), was reported to have a molecular weight of 125 kDa and degree of hydrolysis of 98% (2% acetyl groups). The lignin and PVA were used to prepare aqueous solutions for electrospinning without further purification.

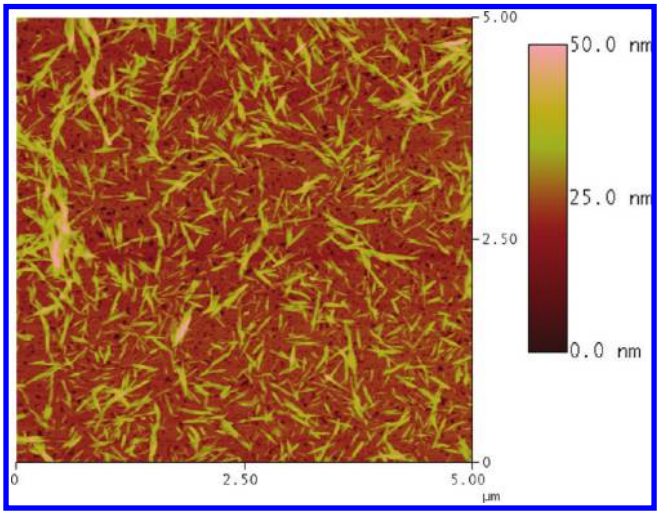


**Figure 1.** AFM height image of cellulose nanocrystals prepared from cotton fibers by acid hydrolysis. The CNCs were spin coated onto a silicon wafer primed with a layer of polyethyleneimine.

Cellulose nanocrystals (CNCs) were prepared by acid hydrolysis from pure cotton (Figure 1). Briefly, cotton was first acid hydrolyzed with 65 wt % sulfuric acid at 50 °C for 20 min. The resulting dispersion was poured into ∼500 g of ice cubes and washed with distilled water until neutral pH by successive centrifugation at 12000 rpm (10 °C, 20 min). Finally, dialysis for 1 week against deionized water with 12000 MWCO membrane was performed to remove trace amounts of residual sulfuric acid from the suspension.

The dimensions of the obtained CNCs (Figure 1) were typically 100−150 nm in length and 10−20 nm in width, in agreement with values reported in the literature.[31,32] The obtained CNC suspension was sonicated for 15 min to avoid aggregation of CNCs and kept refrigerated at 4 °C until use. The concentration of CNCs in the suspension was determined gravimetrically.

**Multicomponent Electrospun Fibers and Solid Films.** PVA aqueous solutions with concentrations ranging from 1.25 to 20 wt % were prepared and given amounts of lignin were added. In addition, aqueous dispersions containing CNC were prepared by using the respective mass ratios of lignin, PVA and CNC. The solutions or suspensions were kept under vigorous mechanical agitation at 60 °C for 15 min, followed by cooling to room temperature under stirring for 120 min. Any given batch of these systems was used to produce electrospun fibers or thin films after no more than 1 week storage time.

The suspensions were loaded into a 10-ml plastic, disposable syringe with a 22 gauge needle. The needle was connected to the positive terminal of a voltage generator, which generated positive voltages up to 50 kV DC (Glassman High Voltage, Series EL). An operating voltage of 19 kV and a flow rate of 8 μL/min (by a computer-controlled syringe pump) were used in typical electrospinning experiments. An aluminum plate of 15 cm diameter covered with a thin aluminum foil and connected to the negative electrode of the power supply (ground) was used as a collector. The working distance was adjusted to 22 cm. Electrospinning was performed at room temperature and at a relative humidity between 35 and 45%. The collected electrospun mats were kept in a desiccator containing anhydrous $CaSO_4$. Solvent-casting was applied in the production of multicomponent solid films. To this end, the solutions or suspensions were poured onto a clean Teflon plate, kept in a dust-free atmosphere, and allowed to dry overnight at room temperature.

**Conductivity, Surface Tension, and Viscosity.** Conductivity and surface tension of the respective solutions or suspensions were measured at room temperature using a conductivity meter (Cornig Inc., model 441) and an electrobalance (CAHN, DCA-312), respectively. The viscosity was determined at 25 °C by a programmable rheometer (TA Instruments, AR2000), as a function of shear rate over a range of 0.1−1000 $s^{-1}$ in a parallel plate configuration (40 mm diameter geometry).

**Fiber Characterization.** The morphology of the nanofibers in the electrospun mats was examined using a field emission scanning electron microscope (FE-SEM, JEOL, 6400F) operating at 5 kV and a working distance 20 mm. A small piece of the nanofiber mat was fixed on carbon tape and then sputtered with Au/Pd. The diameter distribution was obtained from 40 fibers that were selected randomly and image-analyzed (Revolution software).

Fourier transform infrared spectroscopy (FT-IR) was used to investigate the basic chemical characteristics of the electrospun mats. A Nicolet FT-IR spectrometer (Thermo Scientific) was used in the transmittance mode. The multicomponent electrospun mats were dried overnight at 40 °C under vacuum and then grounded with KBr. During any intermediate preparation procedure the samples were maintained in desiccators containing anhydrous $CaSO_4$ to maintain a moisture-free environment. All spectra were collected with a 4 $cm^{-1}$ wavenumber resolution after 64 continuous scans.

Thermogravimetric analyses were performed using TGA (Q500 TGA, TA Instruments) with 10 mg of sample mounted in a platinum pan and heated from 30 to 600 °C at a rate of 10 °C/min under a $N_2$ atmosphere. Additional thermal properties were determined with a differential scanning calorimeter (DSC Q100, TA Instruments) by following two different procedures. In the first set of experiments, 5 mg of the "as produced" fiber mats was placed in the DSC cell and heated from −50 to 250 °C using a 10 °C $min^{-1}$ heating rate. In the other experiments, the fiber mats were heated up to 160 °C and maintained at this temperature for 5 min, followed by cooling down to 0 °C (10 °C/min cooling rate), then heated again to 240 °C (10 °C/min heating rate). The melting temperature ($T_m$) was taken as the peak temperature of the endotherms in thermograms from both

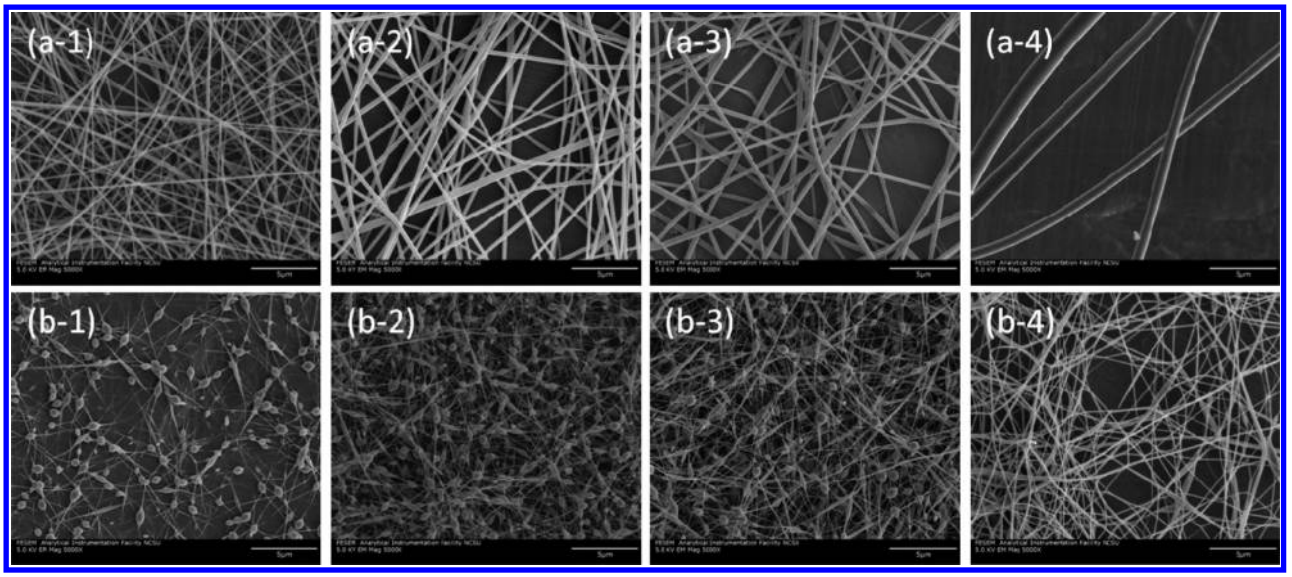


**Figure 2.** Representative FE-SEM micrographs of lignin-based fibers upon electrospinning aqueous solutions containing PVA at concentrations of 10 (upper row, (a) series) and 5% (bottom row, (b) series). The different lignin–PVA mass ratios of the obtained, solid fibers are indicated as follows: 0:100 (1); 20:80 (2); 50:50 (3); and 75:25 (4). The SEM scale bar corresponds to 5 $\mu$m.

experimental procedures. The degree of relative crystallinity ($X_c$) was estimated from the endothermic area using eq 1:

$$X_c(\%) = \Delta H/\Delta H^0 \times 100 \quad (1)$$

where $\Delta H$ is the measured enthalpy of fusion from DSC thermograms and $\Delta H^0$ is the reference enthalpy of fusion for 100% crystalline PVA ($\Delta H^0$ = 158 J g$^{-1}$), as reported in the literature.[33] All the samples used in DSC measurements were dried overnight at 40 °C under vacuum.

## RESULTS AND DISCUSSION

**Bicomponent Electrospun Fibers.** Fiber mats based on lignin and PVA were obtained after electrospinning aqueous dispersions of given compositions. The concentration of lignin in the precursor aqueous solution was varied to obtain fibers with lignin content from 5 to 90 wt % based on solids. Pure lignin solutions did not produce fibers after electrospinning. Figure 2 shows typical SEM images of the electrospun fiber mats (PVA and lignin–PVA) obtained from the aqueous solutions of 10 (Figure 2a series) and 5% (Figure 2b series) PVA concentration. The lignin-free, PVA solution at 10% concentration was readily electrospun and yielded bead-free fibers (Figure 2a-1). Likewise, bead-free and uniform fibers were obtained upon the addition of lignin to this solution (Figure 2a-2–4). Lignin–PVA mixtures of 80:20 mass ratio or higher, were difficult to electrospin due to the onset of phase separation and the significantly high viscosity of the system. In contrast to the case of 10% PVA precursor solution, some beading takes place upon electrospinning lignin-free, 5% PVA solutions (Figure 2b-1). Interestingly, the addition of lignin to these solutions enhances fiber formation (Figure 2b-2–4): a transition from beading to fiber formation occurred as the lignin concentration increased, eventually resulting in bead-free fibers for lignin-PVA mass ratio of 75:25. The enhanced electrospinnability and fiber morphology as lignin is incorporated to the PVA solution is hypothesized to originate by the effect of molecular interactions in the precursor aqueous solution, as will be discussed in other sections of this paper.

In the case of 10% PVA precursor solutions, it is observed that the radius of the fibers increased with lignin addition (see Figure 2a-1–4 and Figure 3), with average values ranging from 61 ± 3 to 509 ± 34 nm.

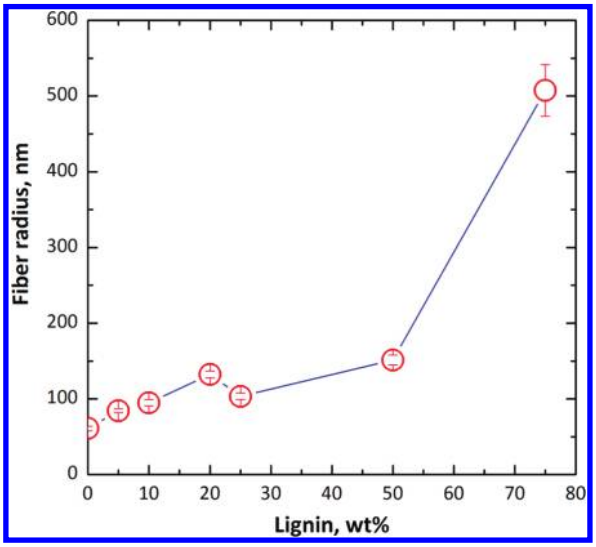


**Figure 3.** Average radius of fibers obtained after electrospinning precursor 10 wt % PVA aqueous solutions before and after loading it with lignin (% lignin in the solid fiber is indicated in the plot; see Figure 2a-1–4). The standard deviations were in most cases smaller than the size of the symbols used. Lines are added as guides to the eye.

The electrospinning process fundamentally requires the transfer of electric charges from the electrode to the spinning fluid at the terminus of the tip. Solutions of low electrical conductivity are subject to insufficient elongation by electrical forces on the fluid jet which is otherwise a condition required to produce uniform fibers.[34–36] In addition, the density of bead-free fibers can be improved by lowering the surface tension of the solution.[34–36] Therefore, we report the electrical conductivity and surface tension (Table 1) as well as the viscosity (Figure 4) of the systems that were more difficult to electrospin, including solutions consisting of 5 or 7 wt % PVA (with and without lignin added).


dx.doi.org/10.1021/bm201828g | Biomacromolecules 2012, 13, 918–926

**Table 1. Electrical Conductivity and Surface Tension of Solutions Based on 5 or 7% PVA Concentration (To Produce Fibers with Lignin Contents of 0−90 wt % Based on Solids)[a]**

| fiber (solid) composition lignin−PVA:% CNC | PVA precursor aqueous solution, wt % | polymer concentration, wt % | conductivity, mS/cm | surface tension, mN/m | morphology |
|---|---|---|---|---|---|
| 0:100/0 | 5.0 | 5.0 | 0.13 | 63.1 ± 0.4 | beads |
| 20:80/0 | 5.0 | 6.2 | 0.17 | 47.5 ± 0.6 | beads + fibers |
| 50:50/0 | 5.0 | 9.5 | 5.24 | 43.2 ± 0.3 | beads + fibers |
| 75:25/0 | 5.0 | 9.5 | 11.89 | 41.6 ± 0.5 | bead-free fibers |
| 85:15/0 | 5.0 | 17.4 | 16.03 | 40.6 ± 0.1 | bead-free fibers |
| 90:10/0 | 5.0 | 34.5 | 20.80 | [b] | no jet |
| 75:25/0 | 5.0 | 17.4 | 11.89 | 41.6 ± 0.5 | bead-free fibers |
| 75:25/5 | 5.0 | 17.4 | 11.76 | 43.2 ± 0.3 | beads + fibers |
| 75:25/10 | 5.0 | 17.4 | 11.84 | 50.8 ± 0.7 | beads + fibers |
| 75:25/15 | 5.0 | 17.4 | 11.93 | 53.7 ± 0.5 | bead-free fibers |
| 20:80/0 | 7.0 | 8.6 | 2.17 | 51.7 ± 2.4 | beads + fibers |
| 20:80/5 | 7.0 | 8.6 | 2.07 | 44.9 ± 0.1 | beads + fibers |
| 20:80/10 | 7.0 | 8.6 | 2.05 | 43.0 ± 1.5 | beads + fibers |
| 20:80/15 | 7.0 | 8.6 | 2.03 | 43.6 ± 1.1 | beads + fibers |

[a]Data for lignin−PVA−CNC dispersions are also included. The composition of the solution is expressed as lignin:PVA mass ratios and % CNC on total solids (lignin:PVA/%CNC), and the morphology of the electrospun systems are indicated. [b]Cannot be measured due to the high viscosity.

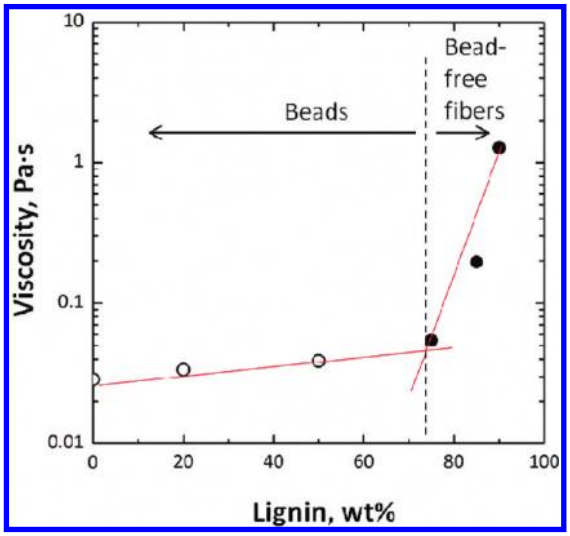


**Figure 4.** Mean apparent viscosity of 5 wt % PVA solutions with different lignin loads (expressed as % lignin in the solid fibers). The viscosity was calculated from the ratio of shear stress and shear rate in the range of 140−550 $s^{-1}$.

The electrical conductivity of the lignin-PVA solutions significantly increased and their surface tension decreased with lignin concentration. Beading upon electrospinning was identified to occur at conductivities lower and surface tensions higher than the respective critical values (≤5.24 mS/cm and ≥43.2 mN/m, respectively; see Table 1 and also Figure 2b-1,2). The viscosity of lignin−PVA solutions increased with the addition of lignin. At about 75% lignin, a steep increase in viscosity with lignin loading is clearly noted (Figure 4). At this concentration, the morphology of the electrospun system changes from beaded fibers to bead-free fibers, as discussed previously. This behavior at the threshold concentration can be explained by the enhanced interaction between PVA and lignin molecules. Overall, it is concluded that lignin−PVA systems can be tuned to facilitate electrospinnability by a proper formulation of the dispersion and, thus, solution properties (mainly electrical conductivity, surface tension, and viscosity).

A ternary phase diagram was constructed after performing electrospinning with a number of lignin−PVA dispersions, as indicated (Figure 5). This ternary diagram helps to better

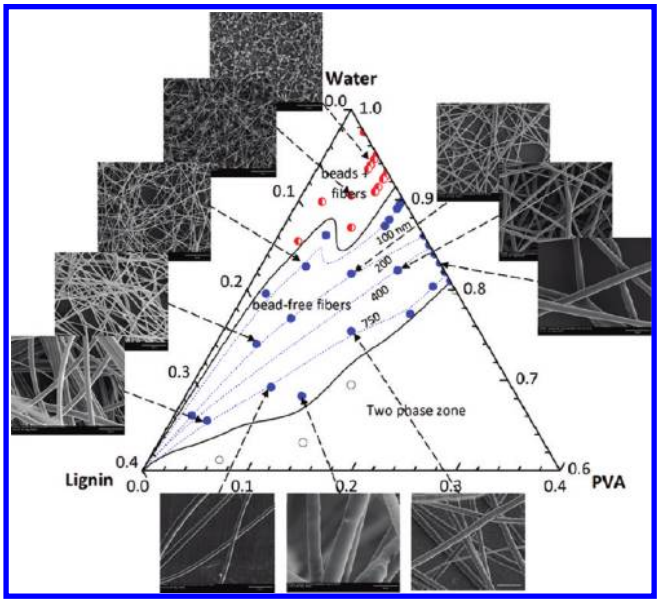


**Figure 5.** Ternary diagram indicating electrospinnability domains according to the composition of the precursor solutions (mass fractions of lignin, PVA, and water). The respective morphology after electrospinning is represented by half-filled circles to indicate beading, filled circles for bead-free fibers, and unfilled circles for a phase separation zone (not suitable for electrospinning). Lines are added as guides to the eye to identify the interfaces between the different domains and iso-radius contour lines are also included according to SEM images of electrospunfibers (representative SEM images are added around the ternary diagram and they include size bars of 5 μm).

identify and predict electrospinnability domains. The relation between solution composition (expressed as mass fractions in the precursor dispersion) and resultant fiber morphologies can be elucidated. Varying composition along a vertical line in the ternary diagram indicates changes in solvent (water) content, which increases as the composition moves closer to the "water"


dx.doi.org/10.1021/bm201828g | Biomacromolecules 2012, 13, 918−926

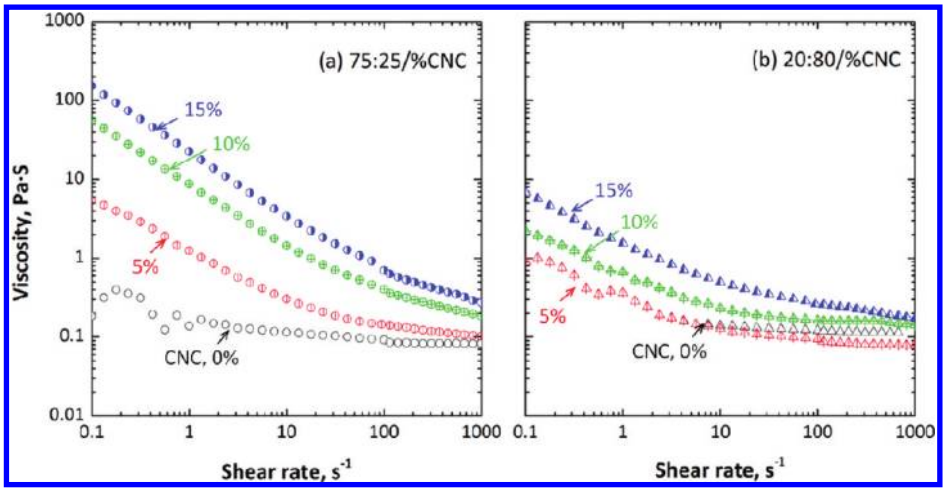


**Figure 6.** Changes in apparent viscosity as a function of the shear rate for lignin−PVA solutions and lignin−PVA−CNC dispersions: 75:25/%CNC (a) and 20:80/%CNC (b). The CNC loading (%CNC) is varied between 0 and 15%, as indicated in the respective plot.

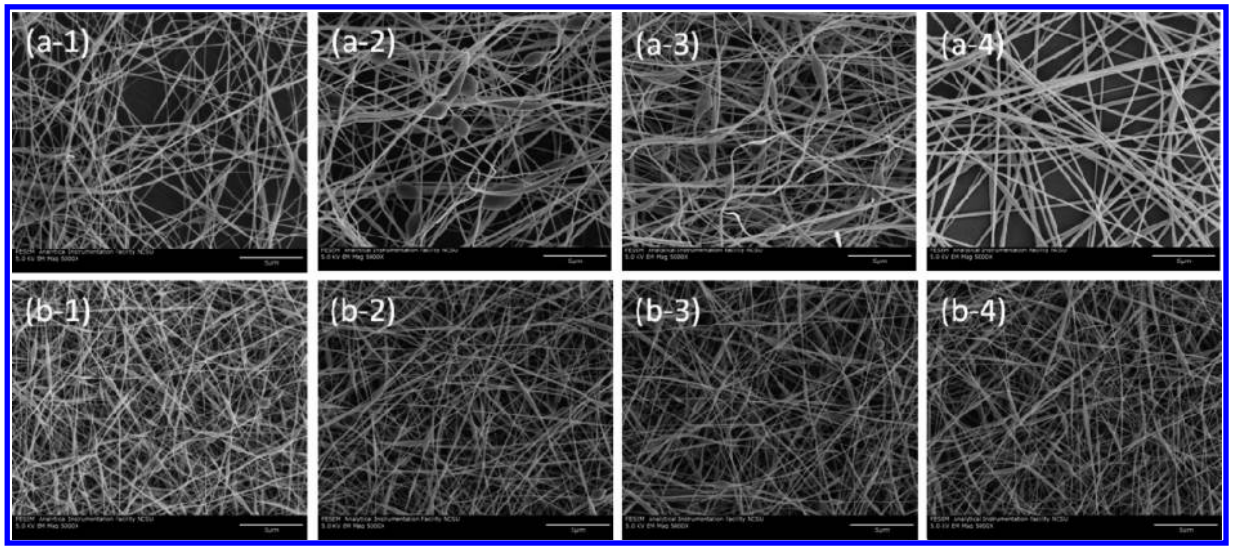


**Figure 7.** SEM images of nanofibers obtained by electrospining lignin−PVA systems (75:25 and 20:80, upper (a) and lower (b) series, respectively) with different CNC loadings (% CNC in lignin−PVA−CNC). Included are reference CNC-free systems (lignin−PVA/0% CNC), 75:25/0 (a-1), or 20:80/0 (b-1), and fibers with 5% CNC loading (lignin−PVA/5%CNC; a-2 or b-2), 10% CNC loading (lignin−PVA/10%CNC; a-3 or b-3), and 15% CNC loading (lignin−PVA/15% CNC; a-4 or b-4).

apex. The changes in the horizontal direction indicate the given lignin:PVA mass ratios.

Three distinctive composition domains were determined, corresponding to (1) beaded fibers, (2) bead-free fibers, and (3) macroscale phase separation. In the latter case, solutions of very high viscosity were obtained and electrospinning failed. Bead-free fibers were observed within a range of component concentrations in precursor solutions between 0 and 32% (lignin), 2 and 19% (PVA), and 66 and 86% (water), respectively. It was found that the diameter of the electrospun fibers increased with the total polymer concentration. High lignin loading was required to produce bead-free fibers. This is an interesting observation because usually PVA is regarded as a good fiber-forming polymer while lignin is not; yet, the synergistic effect when the two components are mixed is apparent (see also Figure 2). Contour lines corresponding to iso-radius were drawn. To the best of our knowledge, such a ternary diagram is reported here for the first time to identify electrospinnability domains.

**Multicomponent Electrospun Fibers.** CNCs were used to produce multicomponent (lignin−PVA−CNC) nanofibers of different compositions. The concentrations of lignin and PVA are given as relative mass fraction in the respective fiber and the % of CNC is given based on total solids. The composition is thereafter represented by "lignin/PVA/%CNC" to indicate the mass ratio between lignin and PVA and the % CNC based on total solids. Lignin−PVA−CNC fiber−precursor dispersions are discussed in more detail in the following sections, but for brevity, only two of the many lignin−PVA compositions tested are described as far as fiber formation, specifically, we focus on dispersions with mass ratios of the matrix system (lignin−PVA) of 75:25 and 20:80 (and 5, 10, and 15% CNC loading based on total solids).

We examine the role of the interactions between the dispersed CNCs and the lignin−PVA medium by measuring the apparent viscosity of the dispersions as a function of the shear rate $\gamma$ (Figure 6). The results indicate a non-Newtonian behavior that is well described by a power law relationship between shear stress ($\tau$) and shear rates ($\gamma$),[37] $\tau = k\gamma^c$, yielding a

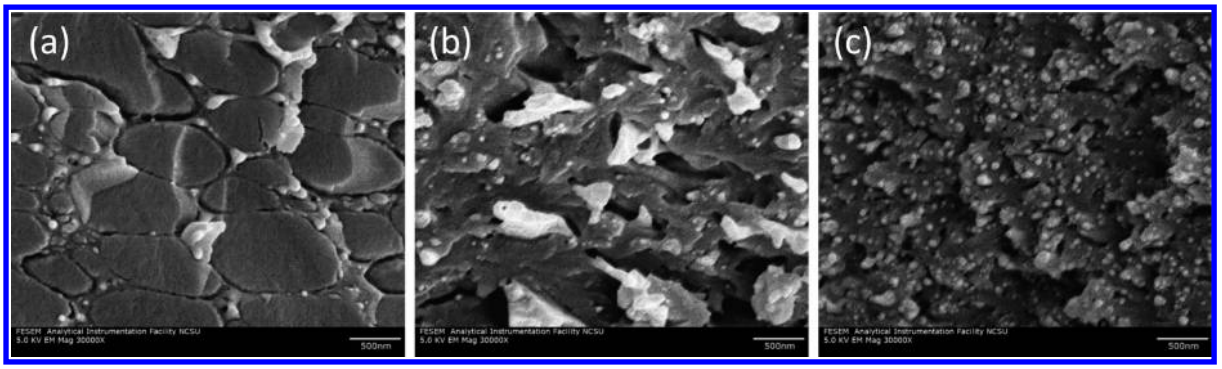


**Figure 8.** Scanning electron microscopy of the cross-section of solid thin films produced from lignin−PVA−CNC systems prepared by evaporation-casting. The specimens were prepared by a freeze fracturing method using liquid nitrogen. Shown are the films with three CNC loadings, that is, lignin−PVA/%CNC of 75:25/0% (a), 75:25/5% (b), and 75:25/15% (c).

power-law index $c$ between 0.26 to 0.89 (shear thinning) and a consistency coefficient $k$ from 0.15 to 20.

The viscosity of the precursor suspensions (lignin−PVA) increased with addition of CNC, which was more evident in the case of 75:25/%CNC systems. There are abundant experimental and theoretical studies which have shown that the viscosity of dispersions of polymers filled with nanoparticles increases with the content of the dispersed phase (and also becomes more shear-thinning).[38−42] In fact, when sheared at low shear rates these systems are highly viscous and gel-like due to the network that is formed. This observation highlights the strong interaction that exists between CNCs and lignin, which is the principal component in 75:25 (lignin−PVA) systems. A significant shear-thinning behavior is observed and explained by the fluctuating structure of the dispersion which is disrupted under shear which produces CNC alignment along the flow direction. In fact, the viscous 75:25/%CNC lignin−PVA−CNC suspensions becomes less viscous under increased shear rates; interestingly, the viscosity of the dispersions decreased asymptotically until reaching values close to the corresponding base, CNC-free lignin−PVA solutions at 1000 $s^{-1}$.

The morphology of the multicomponent fibers produced from 75:25/CNC systems was significantly influenced by the presence of CNCs (see Figure 7a series for 0, 5, 10, or 15% CNC based on total solids). Fibers with a typical radius of 73 ± 5 and 114 ± 4 nm were obtained at the lowest and highest CNC concentrations tested, 5 and 15% CNC, respectively. More specifically, an increase in fiber radius is observed with the addition of CNC. In addition, a few beads were observed at the lower CNC loadings. The shapes of the beads changed from spherical to spindle-like as the concentration was increased from 5 to 10%. Furthermore, considering Figure 6a and Figure 7a series, it can be inferred that more uniform multicomponent fibers are produced with highly shear-thinning dispersions.

In 75:25/%CNC systems the interaction between the CNCs and lignin is expected to dominate. Both the surface tension (Table 1) and viscosity (Figure 6a) are observed to increase with CNC loading. The increase in surface tension of the suspension favors beading while the increase in viscosity favors bead-free fibers.[35] It is apparent that, for dispersions with 15% CNCs, viscous effects are dominant.

In the systems with PVA as the principal component (20:80/%CNC systems), beaded fibers were obtained in all 20:80/% CNC systems (Figure 7b series). Noticeably, upon the addition of CNCs the surface tension decreases (Table 1) and the viscosity increases (Figure 6b); however, compared to 75:25 systems, these changes are more limited and do not substantially influence the resulting fiber morphologies. Overall, the observed changes in the multicomponent nanofibers upon addition of CNCs depend on a complex balance of effects brought about by the dispersed nanoparticles. Importantly, the viscosity and observed morphology results support the hypothesis that a strong interaction exists between CNCs and the lignin phase.

Electrospining is an extremely rapid process where solvent evaporation occurs with continuous jet flow, resulting in the formation of an outer polymer layer and the quenching of the polymer matrix structure.[15−17,43] Nevertheless, further insight into the effect of CNCs on the molecular interactions between lignin and PVA can be gained from solid thin films prepared by the evaporation-casting method. In this process, the characteristic times are much higher due to the slow rates of solvent evaporation, leading to final conditions that are closer to equilibrium. Figure 8 includes SEM images for such films where large phase-separated domains (with characteristic sizes of the order of 500−1000 nm) can be observed for CNC-free systems (Figure 8a). When CNCs are loaded in the system, the characteristic domain size is reduced or suppressed (Figure 8b,c). In general, phase separation occurs during evaporation of highly concentrated polymer solutions.[44] The phase-separated polymer usually evolves into domains with spherical shapes due to the effect of interfacial tension. However, phase separation is prevented if the molecular mobility of the dispersed polymer is much lower than the evaporation rate of the solvent. This effect is hypothesized to occur in the present systems after addition of CNCs: the molecular mobility of the lignin−PVA matrix is decreased with the addition of CNCs, and therefore, phase-separation is reduced.

We now turn our attention to the chemical characterization of electrospun mats produced from the multicomponent systems discussed so far. FT-IR spectra of lignin-based fibers as well as solid film prepared from a CNC suspension were recorded under transmittance mode (Figure 9). As a reference, a pure CNC solid film was prepared by evaporation-casting from 5 wt % CNC aqueous suspension. Characteristic absorbance peaks of lignin at 1598, 1267, 1219, 1130, and 1037 $cm^{-1}$ were assigned respectively to the aromatic skeletal vibration, C−O of guaiacyl ring, C−C and C−O stretch, aromatic C−H in plane deformation in guaiacyl ring, and aromatic C−H in plane deformation.[45] Typical absorbancies for cellulose were assigned to wavenumbers of 1316, 1161, and


dx.doi.org/10.1021/bm201828g | *Biomacromolecules* 2012, 13, 918−926

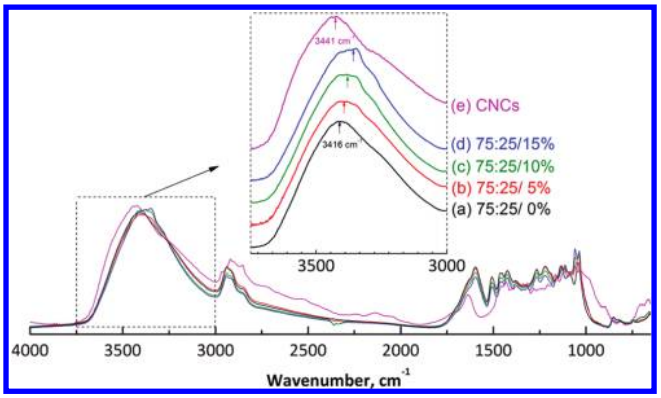


**Figure 9.** FT-IR spectra for electrospun lignin−PVA−CNC mats with different CNC content: lignin−PVA/%CNC of 75:25/0% (a), 75:25/5% (b), 75:25/10% (c), and 75:25/15% (d). A reference film consisting of pure CNC is also included (e).

1059 $cm^{-1}$ for the $CH_2$ vibration, C−O−C asymmetric valence vibration, and C−O valence vibration, respectively. These peaks correlated with the CNC content in the respective system. Most importantly to the present discussion is the observation that compared to CNC-free matrices, fibers with increased amounts of CNCs yielded a shift of the main OH peak region of about 3400 $cm^{-1}$ to lower wavenumbers. This can be explained by the strong hydrogen bonding interactions between the hydrophilic CNC particles and the lignin and PVA medium. Further support for this hypothesis is provided by the shape of the broad absorbance peak between 3550 and 3200 $cm^{-1}$, which is characteristic of OH stretching from the inter- and intramolecular hydrogen bonds.[9,46] The shape of this band is substantially different for samples with or without CNC present. Kraft lignin is a polyphenolic compound containing substituted aromatic groups with different functions ranging from hydroxyl (phenolic or alkyl), conjugated double bond, and methoxyl groups.[47] Therefore, it is expected that some of these functional groups can participate in hydrogen bonding with the hydroxyl groups on the surface of CNCs.

Sulfate groups were grafted onto the surface of CNCs during acid sulfuric acid-catalyzed hydrolysis. The amount of such groups estimated from elemental analysis was about 0.7%, which according to the surface area of the CNC nanoparticles, corresponds to a surface charge density of about 0.30 e/$nm^2$.[48] Thus, the surface density of sulfate groups on the CNCs is relatively small compared to the total available hydroxyl groups. Therefore it is reasonable to expect that the interactions between dispersed CNCs and the lignin/PVA matrices are mainly ascribed to the contribution of hydroxyl groups in hydrogen bonding.

Figure 10 shows thermogravimetric profiles and their derivatives for multicomponent electrospun mats of different CNC content (the curves for pure CNC are included as a reference in the inset of Figure 10). For the weight loss derivative, a sharp and a broad degradation peak are observed for CNC-free mats (lignin−PVA ratio of 75:25, Figure 10d) centered at around 233 and 308 °C, respectively. These peaks correspond to the thermal decomposition of PVA and lignin, respectively. The melting point of pure PVA is 220 °C and the first degradation signal corresponds to chain-stripping reaction produced by the removal of water molecules (dehydration of PVA polymers).[49,50] Lignin decomposition is observed over a broad temperature range and a residue at 500 °C equivalent to

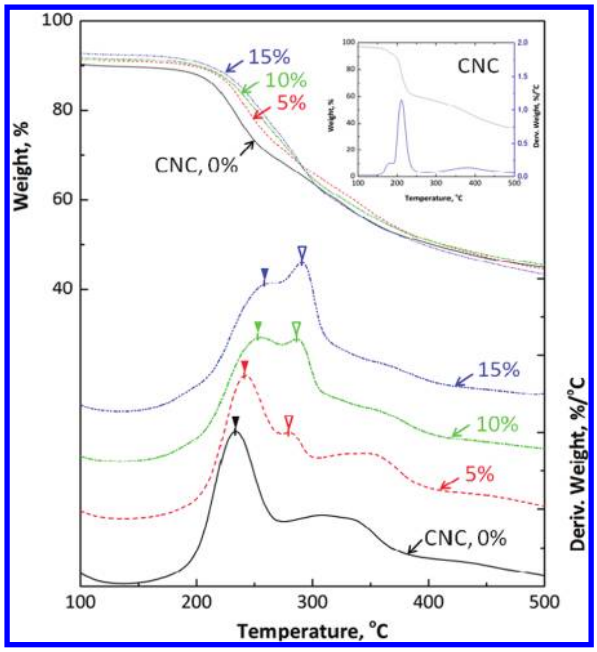


**Figure 10.** Thermogravimetric curves and derivatives of lignin−PVA−CNC electrospun mats with different CNC content. Indicated are the systems consisting of lignin−PVA/%CNC of 75:25/0% CNC (a), 75:25/5% CNC (b), 75:25/10% CNC (c), and 75:25/15% CNC (d). The inverted triangles in the figure show first (filled) and second (open) degradation processes. The inset includes the thermogravimetric profile and derivative of a reference film consisting of pure CNC (100% CNC).

40% of the initial mass is considered unreacted lignin from the composite structure. Some interesting features are observed when cellulose is added to the fibers making the mat. A new peak centered at about 282 °C (unfilled arrow in Figure 10) is identified in the case of CNC-filled systems, which is attributed to cellulose decomposition. This peak is intensified with the addition of CNCs. The degradation peak attributed to pure CNCs at 211 °C was not detected in the CNC-filled systems. Therefore, the addition of CNCs in the matrix system produces better dispersion, as shown in Figure 8, and improves the thermal properties of the composite fibers. The temperature for maximum mass loss of PVA is increased from 233 to 262 °C with the CNC loading of 15%. The suppression of the thermal decomposition of the multicomponent mats could be ascribed to the excellent thermal conductivity of CNC. This property of CNCs has been explained as the result of small phonon scattering in the crystal cellulose chains, which is able to induce more efficient pathway for heat transfer.[51,52]

Returning to our discussion on the increase of fiber radius with the addition of CNC (Figure 7), it is interesting to note that this observation is in contrast with results reported for other nanocomposite systems, including PVA−CNCs.[26,30,52] Such difference can be explained by the intermolecular interactions between the dispersed CNCs and the matrix phase. DSC analyses were performed to investigate the nature of such molecular interactions and Table 2 summarizes the results in terms of the melting temperature and degree of crystallinity. In earlier work, intermolecular interactions between cellulose and PVA were explained on the basis of hydrogen bonding and associated thermodynamic effects.[53,54] A melting point depression can be also caused by morphological effects, such as the reduction of crystalline perfection and the

**Table 2. Melting Temperature ($T_m$) and Degree of Crystallinity ($X_c$) of Electrospun Fiber Mats ("as Produced" and after Isothermal Treatment) for Different CNC Loadings**

| | as produced mats | | | mats after isothermal treatment | | |
|---|---|---|---|---|---|---|
| Lignin:PVA/% CNC | $T_m$ °C | $\Delta H$ J g$^{-1}$ | $X_c$[a] % | $T_{m2}$ °C | $\Delta H_2$ J g$^{-1}$ | $X_c$[a] % |
| 20:80/0 | 221.3 | 120.2 | 76.0 | 217.1 | 65.0 | 41.1 |
| 20:80/5 | 219.3 | 106.5 | 67.4 | 216.7 | 53.5 | 33.9 |
| 20:80/10 | 216.7 | 83.4 | 52.8 | 210.2 | 37.9 | 24.0 |
| 20:80/15 | 216.8 | 69.6 | 44.1 | 211.0 | 31.2 | 19.7 |

[a]The relative crystallinity of PVA in the composite fibers was calculated from the area of melting endotherm on the basis of the heat of fusion of 100% crystalline PVA (158 J g$^{-1}$).

size of the crystallizable polymer, possibly varying with composition in the blends.[55,56] Electrospinning involves extremely rapid solvent evaporation in the continuous jet flow, resulting in thermal quenching of the polymer structure during fiber formation.[15−17,43] Therefore, crystallization of PVA is expected to be induced under nonequilibrium conditions, and kinetic and morpholgical effects are likely to be more dominant than thermodynamic ones.

The melting endotherm of PVA in 75:25 lignin−PVA fibers unfortunately overlapped with the baseline shift as a result of lignin pyrolysis. Thus, only the effect of addition of CNC in 20:80 lignin-PVA systems could be assessed. Therefore, the data in Table 2 corresponds to DSC thermograms of multicomponent lignin−PVA−CNC mats consisting of 20:80/0% (CNC-free fibers), 20:80/5%, 20:80/10%, and 20:80/15%.

For "as produced" (electrospun) fiber mats, an endothermic peak ($T_m$) at 221 °C was observed in CNC-free systems, assigned to the melting of crystalline PVA (Table 2). The corresponding $T_m$ decreased by about 4 °C with addition of CNC at the highest loading (15%). These changes were accompanied by a reduction in the heat of fusion ($\Delta H_m$). Therefore, the degree of crystallinity of PVA estimated from $\Delta H_m$ (eq 1) were calculated to be about 76, 67, 53, and 44% with CNC-free and CNC loading of 5, 10, and 15%, respectively. The suppression of crystallinity of PVA can be explained as the result of the intermolecular interactions between the dispersed CNC particles and the matrix (lignin−PVA), which was also related to the smaller domain sizes observed in Figure 8. In addition, the PVA chains restricted on the surface of CNCs would be less ordered at higher loading of CNCs causing a lower overall crystallinity. This leads to higher excluded volume effects and, as a consequence, the radius of the electrospun fibers increases, as was noted before.

The melting temperature Tm and $\Delta H$ data after thermal treatment at 160 °C (above $T_g$ and near $T_m$) for 5 min are included in Table 2. The data after this thermal treatment show a similar trend in the depression of melting point and crystallinity of the system with increasing CNCs content. This observation may be explained in terms of thermodynamic mixing accompanied by exothermic interaction between a crystalline and an amorphous polymer.[56] Overall, the results suggest that strong intermolecular interactions exist between the CNCs and the matrix consisting of lignin and PVA.

## CONCLUSIONS

Fiber mats were produced from electrospinning dispersions of various compositions containing lignin, poly(vinyl alcohol) (PVA), and cellulose nanocrystals (CNC). The morphology of the multicomponent fibers was examined by SEM and correlated to the phase behavior of the precursor dispersions as well as key properties such as viscosity, electrical conductivity, and surface tension. Ternary phase diagrams were constructed to identify electrospinnability domains and to predict fiber morphology depending on composition. The critical effect of solution rheology was elucidated and the effect of CNC loading was studied. The intermolecular interactions, mainly hydrogen bonding between the polymer matrix and the dispersed CNCs, played an important role. The addition of CNC improved the thermal stability of composite electrospun fibers. Overall, lignin-based fibrous architectures from electrospinning are expected to have great potential for tailoring new functional materials.

## AUTHOR INFORMATION

### Corresponding Author

*E-mail: ojrojas@ncsu.edu.

### Notes

The authors declare no competing financial interest.

## ACKNOWLEDGMENTS

The authors acknowledge financial support of Asahikasei Fibers Coporation, Japan. Tokushima Bunri University is gratefully acknowledged for funding M.A. during her international exchange program with NC State University (O.J.R.).

## REFERENCES

(1) Aden, A. R., M.; Ibsen, K.; Jechura, J.; Neeves, K.; Sheehan, J.; Wallace, B.; Montague, L.; Slayton, A.; Lukas, J. Lignocellulosic Biomass to Ethanol Process Design and Economics Utilizing Co-Current Dilute Acid Prehydrolysis and Enzymatic Hydrolysis for Corn Stover. *NREL/TP-510-32438*; National Renewable Energy Laboratory: Golden, CO, June 2002.

(2) Pu, Y.; Kosa, M.; Kalluri, U. C.; Tuskan, G. A.; Ragauskas, A. J. *Appl. Microbiol. Biotechnol.* **2011**, *91*, 1525−36.

(3) Kadla, J. F.; Kubo, S. *Composites, Part A* **2004**, *35*, 395−400.

(4) Kubo, S.; Kadla, J. F. *Biomacromolecules* **2003**, *4*, 561−567.

(5) Mousavioun, P.; Doherty, W. O. S.; George, G. *Ind. Crops Prod.* **2010**, *32*, 656−661.

(6) Pucciariello, R.; Bonini, C.; D'Auria, M.; Villani, V.; Giammarino, G.; Gorrasi, G. *J. Appl. Polym. Sci.* **2008**, *109*, 309−313.

(7) Hatakeyama, H. Polyurethanes Containing Lignin. In *Chemical Modification, Properties, and Usage of Lignin*; Hu, T. Q., Ed.; Kluger: New York, 2002; pp 41−56.

(8) Kadla, J. F.; Kubo, S.; Venditti, R. A.; Gilbert, R. D.; Compere, A. L.; Griffith, W. *Carbon* **2002**, *40*, 2913−2920.

(9) Kubo, S.; Kadla, J. F. *Biomacromolecules* **2005**, *6*, 2815−2821.

(10) Lallave, M.; Bedia, J.; Ruiz-Rosas, R.; Rodríguez-Mirasol, J.; Cordero, T.; Otero, J. C.; Marquez, M.; Barrero, A.; Loscertales, I. G. *Adv. Mater.* **2007**, *19*, 4292−4296.

(11) Ruiz-Rosas, R.; Bedia, J.; Lallave, M.; Loscertales, I. G.; Barrero, A.; Rodríguez-Mirasol, J.; Cordero, T. *Carbon* **2010**, *48*, 696−705.

(12) Montero, G. A., Peresin, M. S., Rojas, O. J. Lignin in the production nanofibers via electrospinning. 82nd Colloid and Surfaces Symposium, Raleigh, NC, June 15−18, 2008; American Chemical Society: Washington, D.C., 2008.

(13) Dallmeyer, I.; Ko, F.; Kadla, J. F. *J. Wood Chem. Technol.* **2010**, *30*, 315−329.

(14) Reneker, D. H.; Yarin, A. L.; Zussman, E.; Xu, H., Electrospinning of Nanofibers from Polymer Solutions and Melts. In

*Advances in Applied Mechanics*; Hassan, A., Erik van der, G., Eds.; Elsevier: New York, 2007; Vol. *41*, pp 43−346.
(15) Hohman, M. M.; Shin, M.; Rutledge, G.; Brenner, M. P. *Phys. Fluids* **2001**, *13*, 2201−2220.
(16) Shin, Y. M.; Hohman, M. M.; Brenner, M. P.; Rutledge, G. C. *Polymer* **2001**, *42*, 09955−09967.
(17) Reneker, D. H.; Yarin, A. L.; Fong, H.; Koombhongse, S. *J. Appl. Phys.* **2000**, *87*, 4531−4547.
(18) Yoon, K.; Kim, K.; Wang, X.; Fang, D.; Hsiao, B. S.; Chu, B. *Polymer* **2006**, *47*, 2434−2441.
(19) Ding, B.; Kim, J.; Miyazaki, Y.; Shiratori, S. *Sens. Actuators, B* **2004**, *101*, 373−380.
(20) Kim, K.; Yu, M.; Zong, X.; Chiu, J.; Fang, D.; Seo, Y.-S.; Hsiao, B. S.; Chu, B.; Hadjiargyrou, M. *Biomaterials* **2003**, *24*, 4977−4985.
(21) Li, D.; Xia, Y. *Adv. Mater.* **2004**, *16*, 1151−1170.
(22) Zussman, E.; Chen, X.; Ding, W.; Calabri, L.; Dikin, D. A.; Quintana, J. P.; Ruoff, R. S. *Carbon* **2005**, *43*, 2175−2185.
(23) Azizi Samir, M. A. S.; Alloin, F.; Dufresne, A. *Biomacromolecules* **2005**, *6*, 612−626.
(24) Moon, R. J.; Martini, A.; Nairn, J.; Simonsen, J.; Youngblood, J. *Chem. Soc. Rev.* **2011**, *40*, 3941−3994.
(25) Habibi, Y.; Lucia, L. A.; Rojas, O. J. *Chem. Rev.* **2010**, *110*, 3479−3500.
(26) Peresin, M. S.; Habibi, Y.; Zoppe, J. O.; Pawlak, J. J.; Rojas, O. J. *Biomacromolecules* **2010**, *11*, 674−681.
(27) Peresin, M. S.; Habibi, Y.; Vesterinen, A.-H.; Rojas, O. J.; Pawlak, J. J.; Seppälä, J. V. *Biomacromolecules* **2010**, *11*, 2471−2477.
(28) Zoppe, J. O.; Peresin, M. S.; Habibi, Y.; Venditti, R. A.; Rojas, O. J. *ACS Appl. Mater. Interfaces* **2009**, *1*, 1996−2004.
(29) Yao, L.; Haas, T. W.; Guiseppi-Elie, A.; Bowlin, G. L.; Simpson, D. G.; Wnek, G. E. *Chem. Mater.* **2003**, *15*, 1860−1864.
(30) Zhou, C.; Chu, R.; Wu, R.; Wu, Q. *Biomacromolecules* **2011**, *12*, 2617−25.
(31) Ebeling, T.; Paillet, M.; Borsali, R.; Diat, O.; Dufresne, A.; Cavaillé, J. Y.; Chanzy, H. *Langmuir* **1999**, *15*, 6123−6126.
(32) Elazzouzi-Hafraoui, S.; Nishiyama, Y.; Putaux, J.-L.; Heux, L.; Dubreuil, F.; Rochas, C. *Biomacromolecules* **2007**, *9*, 57−65.
(33) Pyda, M. ATHAS database. http://athas.prz.edu.pl/.
(34) Magarvey RH, O. L. *J. Fluid Mech.* **1962**, *31*, 151−157.
(35) Fong, H.; Chun, I.; Reneker, D. H. *Polymer* **1999**, *40*, 4585−4592.
(36) Bhardwaj, N.; Kundu, S. C. *Biotechnol. Adv.* **2010**, *28*, 325−347.
(37) Metzner, A. B.; Otto, R. E. *AlChE J.* **1957**, *3*, 3−10.
(38) Otsubo, Y.; Umeya, K. *J. Rheol.* **1984**, *28*, 95−108.
(39) Shikata, T.; Pearson, D. S. *J. Rheol.* **1994**, *38*, 601−616.
(40) Rahatekar, S. S.; Koziol, K. K. K.; Butler, S. A.; Elliott, J. A.; Shaffer, M. S. P.; Mackley, M. R.; Windle, A. H. *J. Rheol.* **2006**, *50*, 599−610.
(41) Thomin, J. D.; Keblinski, P.; Kumar, S. K. *Macromolecules* **2008**, *41*, 5988−5991.
(42) Jaber, E.; Luo, H.; Li, W.; Gersappe, D. *Soft Matter* **2011**, *7*, 3852−3860.
(43) Bognitzki, M.; Frese, T.; Steinhart, M.; Greiner, A.; Wendorff, J. H.; Schaper, A.; Hellwig, M. *Polym. Eng. Sci.* **2001**, *41*, 982−989.
(44) Shuto, K.; Oishi, Y.; Kajiyama, T.; Han, C. C. *Macromolecules* **1993**, *26*, 6589−6594.
(45) Lin, S. Y. Methods in Lignin Chemistry. In *Springer Series in Wood Science*; Dence, C. W., Ed.; Springer-Verlag: New York, 1992; pp 83−109.
(46) Fengel, D. *Holzforschung* **1993**, *47*, 103−108.
(47) Kringstad, K. P.; Mörck, R. *Holzforschung* **1983**, *37*, 237−244.
(48) Habibi, Y.; Hoeger, I.; Kelley, S. S.; Rojas, O. J. *Langmuir* **2009**, *26*, 990−1001.
(49) Zhao, W.; Yamamoto, Y.; Tagawa, S. *J. Polym. Sci., Part A: Polym. Chem.* **1998**, *36*, 3089−3095.
(50) Gilman Jeffrey, W.; VanderHart David, L.; Kashiwagi, T., Thermal Decomposition Chemistry of Poly(vinyl alcohol). In *Fire and Polymers II*; American Chemical Society: Washington, DC, 1995; Vol. *599*, pp 161−185.
(51) Shimazaki, Y.; Miyazaki, Y.; Takezawa, Y.; Nogi, M.; Abe, K.; Ifuku, S.; Yano, H. *Biomacromolecules* **2007**, *8*, 2976−2978.
(52) Ping, L.; You-Lo, H. *Nanotechnology* **2009**, *20*, 415604.
(53) Nishio, Y.; Haratani, T.; Takahashi, T.; Manley, R. S. J. *Macromolecules* **1989**, *22*, 2547−2549.
(54) Scott, R. L. *J. Chem. Phys.* **1949**, *17*, 279−284.
(55) Nishio, Y.; Haratani, T.; Takahashi, T. *J. Polym. Sci., Part B: Polym. Phys.* **1990**, *28*, 355−376.
(56) Nishi, T.; Wang, T. T. *Macromolecules* **1975**, *8*, 909−915.